PERGAMON

International Journal of Heat and Mass Transfer 45 (2002) 3571–3583

International Journal of HEAT and MASS TRANSFER

www.elsevier.com/locate/ijhmt

Turbulent transport from continuous sources at the wall of a channel

Dimitrios V. Papavassiliou *

School of Chemical Engineering and Materials Science, The University of Oklahoma, 100 East Boyd St., SEC T335, Norman, OK 73019, USA

Received 16 July 2001; received in revised form 1 February 2002

Abstract

Dispersion from a continuous line source located at the wall of a turbulent channel and transport over a step change in wall heat flux are studied for fluids with Prandtl numbers between 0.1 and 2400. Direct Numerical Simulation is used to develop the velocity flow field, which is then coupled with a particle tracking algorithm to describe the behavior of heat or mass markers released from instantaneous sources on the wall. The positions in time and space of these markers, which have been available as a database created by Papavassiliou and Hanratty [Int. J. Heat Mass Transfer 40 (6) (1997) 1303], are used as the building block for the study of passive scalar transport from the wall of the channel. Qualitative and quantitative results are obtained with particular emphasis on transport parameters from the wall.

1. Introduction

Turbulent scalar transport plays a crucial role in a number of diverse applications such as the design of heat exchange equipment, the design of reactors and mixing tanks, and the dispersion of pollutants in the atmosphere. Specifically, turbulent transport at very low Prandtl, *Pr*, number fluids has applications in liquid metal heat transfer. High Prandtl or Schmidt number transport is important in lubrication and even higher Schmidt, *Sc*, numbers are found in electrochemical applications for semiconductor manufacturing.

The development of methodologies for the Direct Numerical Simulation (DNS) of turbulent flows in the last 15 years allowed the possibility to shed new light on the fundamental phenomena that govern turbulent transport [1]. On the other hand, DNS is limited by the capabilities of high performance computers to simulations in relatively simple geometries and low Reynolds numbers. In the case of heat transfer, DNS has been implemented for a relatively narrow range of fluids (*Pr* between 0.025 and 10) [2–7]. Each one of these simulations described a specific configuration of the transport problem (i.e. isothermal walls or constant heat flux walls). Laboratory studies have been conducted [8] that replicated and validated the DNS virtual experiments. The restriction in the range of *Pr* or *Sc* arises from the fact that in order to resolve all the scales of motion and temperature, the number of grid points has to be analogous to $Pr^{3/2}Re^{9/4}$. Furthermore, at high *Pr*, the temperature gradient close to the wall is very steep and an Eulerian simulation would require very small time steps and very fine resolution; the computational cost is prohibitive. At low *Pr* the mean temperature gradient, $\mathrm{d}\bar{T}/\mathrm{d}y$, in the center region of the channel has a finite and significant value (for the case of heat transfer from a hot wall to a cold wall and isothermal boundaries). The temperature fluctuation production term, $\overline{v\theta}\mathrm{d}\bar{T}/\mathrm{d}y$, has a large value at the center of the channel. It follows that the center region of the channel should be very finely resolved in addition to the wall region, which restricts the lower *Pr* possible. Isoflux boundary conditions, that result in flat mean temperature profiles at the center of a channel, can be used for DNS of low *Pr* fluids but cannot eliminate the restriction of an upper *Pr*. Experiments are easily done for isothermal walls [8,9]. The Lagrangian Scalar Tracking technique, however, has been used [10] to reconstruct first-order statistics for *Pr*

* Tel.: +1-405-325-0574; fax: +1-405-325-5813.
E-mail address: dvpapava@ou.edu (D.V. Papavassiliou).

0017-9310/02/$ - see front matter
PII: S0017-9310(02)00065-0

Nomenclature

A	constant in the power law relation for the heat transfer coefficient
C	concentration
$c_1,\ c_2$	coefficients in the power law relation for the ground level temperature downstream from a continuous line source (see Eq. (12))
C_p	specific heat at constant pressure
D	diffusivity
E_c, E_v	eddy conductivity, eddy viscosity
h	half channel height
K	heat transfer coefficient
k	thermal conductivity
m	exponent in the power law relation for the heat transfer coefficient
Nu	Nusselt number ($Nu = Kh/k$)
P_1	conditional probability of a marker being at a location (x, y) at time t, given that it was released at a known time from a known location at the wall
P_2	joint probability of a marker being at a location (x, y)
P_3	marginal probability of a marker being at a distance y from the wall
P_4	probability of a marker being at a distance y from the wall at $x = x_1$
Pr	Prandtl number $\left(Pr = \frac{\nu}{\alpha}\right)$
q	heat flux
R^L	Lagrangian correlation coefficient
Re	Reynolds number $\left(Re = \frac{U_c h}{\nu}\right)$
Sc	Schmidt number $\left(Sc = \frac{\nu}{D}\right)$
St	Standon number $\left(St = \frac{Nu}{Re\,Pr}\right)$
T	temperature
t	time
$\vec{U}$	Eulerian velocity vector
u, v, w	fluctuating velocity components in the x, y, z directions
$\vec{V}$	Lagrangian velocity vector
x, y, z	streamwise, normal and spanwise coordinates
X	displacement of a marker from the source in the x direction
$\vec{X}$	position vector of a marker
$\vec{x_0}$	initial position vector of a marker

Greek symbols

α	thermal diffusivity
δ_d	boundary layer displacement thickness $\left(\delta_d = \int_0^\infty \left(1 - \frac{U}{U_c}\right) dy\right)$
δ_T	thermal layer thickness
Δt	time step
$\Delta x, \Delta y$	bin size in the x and y directions
θ	temperature fluctuation
λ	lateral half plume width
ν	kinematic viscosity
ξ	dimensionless distance from the wall based on λ
ρ	fluid density
σ	standard deviation of a probability density function
τ_w	shear stress at the wall

Superscripts and subscripts

$\overline{()}$	ensemble average
$()^L$	Lagrangian variable
$()^+$	value made dimensionless with the wall parameters
$()^*$	friction value
$()_1$	value upstream from the thermal region
$()_c$	value at the center of the channel
$()_{max}$	maximum value
$()_o$	value at the instant of marker release
$()_w$	value at the wall of the channel

as high as 2400. Another advantage of this Lagrangian technique is that information from one computation can be used to reconstruct the behavior in different problem configurations: isothermal and isoflux walls, step change in wall temperature or heat flux, continuous or instantaneous line source behavior.

The contributions of the present paper can be summarized as: (a) the presentation of a computational method that can be used to calculate transport properties, which is based on the velocity field but does not use the Reynolds analogy, and (b) the study of turbulent heat/mass transfer from continuous wall sources in a wide range of molecular Prandtl or Schmidt numbers (liquid metals, cryogenic fluids, refrigerants, air, and electrolytic fluids).

2. Background

2.1. Turbulent transport of heat or mass in an Eulerian framework

In an Eulerian description of turbulent transport, the temperature [1] is decomposed as $T = \bar{T} + \theta$. The temperature can become dimensionless using the friction temperature T^*, $T^* = (q_w)/(\rho C_p u^*)$, where q_w is the heat

[1] The scalar quantity used in this paper is the temperature and the dimensionless number is the Prandtl number. The results can be applied directly to the case of turbulent mass transfer without chemical reaction by replacing temperature with concentration and Prandtl number with Schmidt number.

flux at the wall defined in terms of the thermal conductivity k as $q_w = -k(d\bar{T}/dy)_w$. The dimensionless temperature in wall units, T^+, is then defined as

$$T^+ = \frac{T}{T^*} = -\frac{T\rho C_p u^*}{(k(d\bar{T}/dy))_w} = -Pr\frac{T}{(d\bar{T}/dy^+)_w}, \quad (1)$$

where y^+ is the distance from the wall in viscous wall units ($y^+ = yu^*/\nu$). In a fully developed state, the heat flux is constant through the channel and a dimensionless heat transfer coefficient, K^+, can be defined as $K^+ = K/(\rho C_p u^*)$ with K given by

$$q_w = K(\overline{T_c} - \overline{T_w}), \quad (2)$$

where $\overline{T_c}$ is the mean temperature at the center of the channel and $\overline{T_w}$ is the mean temperature at the wall. The above equations and definitions can be used to derive the following relation:

$$K^+ = \frac{1}{Pr}\left[\frac{d(\bar{T}/(\overline{T_c} - \overline{T_w}))}{dy^+}\right]_w. \quad (3)$$

At high Pr, the thermal layer is very thin and the velocity field inside it can be described using a Taylor series expansion in terms of the dimensionless distance from the wall y^+. The analogy between momentum and heat or mass transfer predicts that the eddy conductivity is given as $E_c^+ \sim y^{+n}$, where n is an integer greater than or equal to 3, which results to a power law relation for K^+ [11]

$$K^+ = APr^m. \quad (4)$$

2.2. Lagrangian turbulent transport

Einstein [12] developed a relation that describes the dispersion of fluid particles in a non-turbulent field in terms of the mean-squared displacement from the source in the x direction:

$$\frac{d\overline{X^2}}{dt} = 2D, \quad (5)$$

where D is the molecular diffusivity. Taylor [13] developed a similar relation for the dispersion of fluid particles from a point source in homogeneous, isotropic turbulence:

$$\frac{d\overline{X^2}}{dt} = 2\overline{u^2}\int_0^t R^L(\tau)d\tau, \quad (6)$$

where $\overline{u^2}$ is the mean-square of the x-component of the velocity of the fluid particles and R^L is the Lagrangian correlation coefficient. An important implication of Eq. (6) is that the history of the particle motion affects the rate of dispersion through R^L. Dispersion of heat or mass markers introduces an additional complication, since the markers can move off of a fluid particle as a result of molecular diffusion. Saffman [14] developed a relation for dispersion in this case by defining a material autocorrelation function, which differs from the Lagrangian correlation in that it correlates fluid velocity components along the trajectories of markers instead of fluid particles.

Hanratty [15] used Taylor's theory to describe the transfer of heat in turbulent channel flow. An infinite number of line sources of heat along one wall was used to describe the hot plane and an infinite number of line sinks of heat along the other wall described the behavior of the cold plane. A clearer physical picture for heat transport emerged through this approach. The variation of the eddy conductivity with the distance from the wall was associated with the time dependency of turbulent diffusion [16]. Temperature gradients close to the wall were found to result from thermal markers that had been in the field for small periods of time. This analysis assumed a homogeneous and isotropic velocity field. Information about the behavior of such wall sources is needed in order to use Lagrangian methods to describe Eulerian temperature fields in other, more realistic situations. There are such investigations in the literature (see [17–22]) that have carried out experimental studies of wall sources. However, none of these studies give the space–time behavior of an instantaneous source and only the study of Incropera et al. [21] examines transport in a fully developed channel flow.

3. The Lagrangian scalar tracking approach

A Lagrangian approach is a natural way to describe transport and it can provide valuable physical insights. This work extends the use of Lagrangian methods to study the transfer of heat in flows with continuous sources of heat at the wall of a channel and with a step change in the heat transfer flux from the wall of a channel. The stochastic particle tracking technique is described in a thesis by Kontomaris [23], where more detailed information regarding the numerical method can be found. Kontomaris and Hanratty [24] have used Lagrangian tracking to study the behavior of fluid particles released in the center of a turbulent channel flow. The complete methodology, which includes the stochastic tracking of heat or mass markers along with the statistical post-processing of the results to obtain scalar profiles, will be referred to as the *Lagrangian Scalar Tracking* (LST) method. It has also been implemented by another laboratory for the simulation of mass transfer in low Re fluids and non-Cartesian geometry for bubble dissolution in the presence of surfactants and $Sc = 500$ [25].

3.1. Marker tracking

The velocity field of a Newtonian and incompressible fluid was calculated using a DNS of fully developed

turbulent flow in a channel [3,6,26]. The flow was regarded periodic in the streamwise and spanwise directions, with periodicity lengths equal to the size of the computational box in these directions ($4\pi h \times 2h \times 2\pi h$ in x, y, z, where $h = 150$). Numerical experiments at $Re = 2660$ were conducted. The resolution for the runs was $128 \times 65 \times 128$. The accuracy of these simulations has been validated and documented by a comparison with laboratory measurements at the same conditions [3,27].

In the Lagrangian framework, the system of reference moves with the fluid particles, or the heat or mass markers in the case of turbulent heat or mass transport. The trajectories of such heat or mass markers released from the wall can be calculated in the hydrodynamic field created by the DNS with a particle tracking method [28]. The basic assumption is that a heat marker at each time has the velocity of the fluid particle that carries it, $\vec{V}(\overrightarrow{x_0}, t) = \vec{U}$, where $\vec{V}(\overrightarrow{x_0}, t)$ is the Lagrangian velocity of a marker that was released at location $\overrightarrow{x_0}$ and $\vec{U}$ is the Eulerian velocity of the fluid at the location of the marker at time t. The equation of particle motion then is

$$\vec{V}(\overrightarrow{x_0}, t) = \frac{\partial \vec{X}(\overrightarrow{x_0}, t)}{\partial t}. \tag{7}$$

The equation of particle motion was integrated using an Adams–Bashforth scheme. Each marker moved due to two effects, the convective effect and the molecular effect. The convective part was calculated from the fluid velocity at the particle position. A mixed sixth-order Lagrangian–Chebyshev interpolation scheme was used to calculate the velocity vector between grid points. The effect of molecular diffusion was simulated by imposing a 3D random walk on the particle motion; it was added on the convective part of the motion after each time step and it took values from a Gaussian distribution with zero mean and standard deviation $\sigma = \sqrt{(2\Delta t/Pr)}$ in wall units. This follows from Einstein's theory for Brownian motion (see Eq. (5)). Using this methodology, the Prandtl number does not limit LST. Note also that the presence of these markers does not affect the flow field, so that the behavior of a passive scalar was simulated.

The results presented here use the database created by Papavassiliou and Hanratty [10]. Two sets of tracking experiments were performed. In the first set, Prandtl numbers of $0.1, 1, 10$ and 100 were studied with 16,129 markers released instantaneously for each Pr in the same velocity field. The initial position of the markers was on a uniform grid that covered the bottom wall of the channel. No more than one marker was released from each cell in order to avoid the introduction of markers with highly correlated initial conditions. In the second set, a different velocity field was used to start the calculations. The two initial hydrodynamic fields were flow realizations that were 2750 wall time units apart, which is longer than the longest Eulerian time scale in this type of flow, in order to acquire statistically non-correlated samples. The number of markers and their initial locations were the same as in the first set of runs. However, the Prandtl numbers were $0.7, 1, 3, 500$ and 2400. The second run at $Pr = 1$ was conducted in order to estimate the statistical variations of the results and to assess the effect of different initial velocity fields. It was found that the difference in the statistical behavior of the two $Pr = 1$ runs was less than 1%. Each set of computer experiments was carried out on one processor of a CONVEX C3880 supercomputer and for up to 2750 wall time units. The computational time was in the order of 27 Service Units per 500 iterations with $\Delta t = 0.25$; tracking 16,129 markers for each Pr required about 10% of the computational time that was required for the hydrodynamics DNS. The criterion to terminate the tracking was statistical. The walls of the channel confine the motion of the markers and force the probability function, P, to find a marker at a distance y from the wall to become uniform. At stationary state, the variance of P should equal that of a uniform distribution between $y = 0$ and $y = 2h$, $\sigma^2 = (2h - 0)^2/12 = 7500$.

3.2. Statistical post-processing

Let $P_1(x - x_0, y, t - t_0 \,|\, t_0, x_0)$ be the joint and conditional probability density function for a marker to be at a location (x, y) at time t, given that the marker was released at x_0 at time t_0. For each experiment, the trajectories of all markers are used as an ensemble to obtain P_1. Since the flow field is homogeneous in the x and z directions, there is no statistical dependence on the initial location of the markers. This probability can be interpreted physically as concentration [29] and, thus, as a snapshot of a cloud of contaminants released instantaneously from $x_0 = 0$. Probability P_1 can be used to extract information about the behavior of a continuous line source at x_0 by integrating over time

$$P_2(x - x_0, y \,|\, x_0) = \int_{t_0}^{\infty} P_1(x - x_0, y, t - t_0 \,|\, t_0, x_0)\mathrm{d}t. \tag{8}$$

The behavior of a heated plane is described with a series of continuous line sources covering the plane. Therefore, the mean temperature profile in a channel, where heat is added to the fluid from the bottom wall at a constant rate (isoflux conditions), can be synthesized from P_2 by integrating P_2 over the streamwise direction

$$\begin{aligned} P_3(y) &= \int_{x_0}^{\infty} P_2(x - x_0, y \,|\, x_0)\mathrm{d}x \\ &= \int_{x_0}^{\infty} \int_{t_0}^{\infty} P_1(x - x_0, y, t - t_0 \,|\, t_0, x_0)\mathrm{d}t\,\mathrm{d}x. \end{aligned} \tag{9}$$

Distribution P_3 can be interpreted physically as the mean temperature profile in a channel with a heated wall,

$\bar{T}(y) = P_3(y)$. The above expression corresponds to the case when a constant number of markers is released at every time step, an isoflux boundary condition.

The behavior of heat transport over a plate that has a step change in heat flux at x_0 can also be synthesized from P_2 as follows

$$\bar{T}(x_1, y) = P_4(x_1, y) = \int_{x_0}^{x_1} P_2(x - x_0, y \,|\, x_0)\mathrm{d}x = \int_{x_0}^{x_1} \int_{t_0}^{\infty} P_1(x - x_0, y, t - t_0 \,|\, t_0, x_0)\mathrm{d}t\,\mathrm{d}x. \quad (10)$$

The physical interpretation of P_4 is that it represents the mean temperature profile at distance $(x_1 - x_0)$ downstream from a step change in heat flux from the wall at x_0.

The total number of markers that are present in the flow field at any time is 16,129. This is the size of the sample space for the calculation of P_1. For the calculation of P_2, which is an integration in discrete time of P_1, the number of markers that are used increases with the number of discrete time steps. The integration to time $t^+ = 2750$ involves the calculation of the position of $16{,}129 \times 2750 = 4.435475 \times 10^7$ markers.

Probability P_2 is calculated for each Pr using a grid that covers the flow domain and counting the markers that are present in each grid cell. The grid in the y direction is constructed either by dividing the width of the channel uniformly in 300 bins (when $Pr \leqslant 100$), or by using Chebyshev collocation points to generate 200 bins (when $Pr > 100$) in order to increase the resolution closer to the wall. In the x direction, the grid is stretched, in order to take measurements at long distances downstream from the source. The stretching in the x direction followed the relation $\Delta x_n = 1.06^n \Delta x_{(n-1)}$ with $\Delta x_0 = 5$ in wall units.

4. Results

4.1. Behavior of a continuous line source at the wall

Fig. 1 presents a comparison of our LST results with measurements by Poreh and Cermak [17] presented in Poreh and Hsu [18] for the mean concentration profile downstream from a continuous line source at the wall in a turbulent boundary layer. The experiments involved the diffusion of a scalar quantity (ammonia gas in air, $Sc = 0.7$) from a steady line source within a turbulent boundary layer. The scaling in the figure follows Poreh and Cermak's suggestion to scale the concentration with the maximum concentration, $C_{\max}$, and the distance from the wall with the lateral plume half-width, λ, which is defined from the following:

$$\frac{C}{C_{\max}} = f(\xi), \quad (11)$$

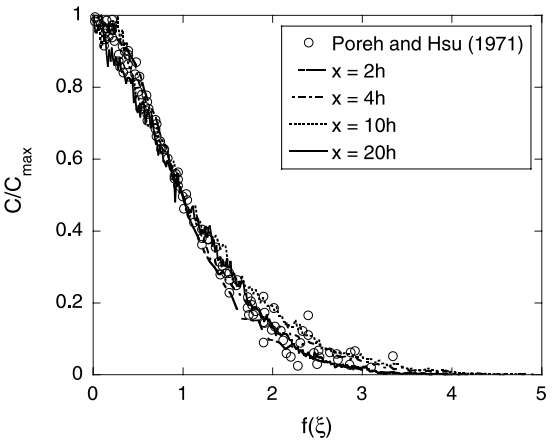

Fig. 1. Comparison of the Lagrangian simulation results (shown as lines) for the concentration profiles downstream from a continuous line source with measurements by Poreh and Hsu [18] in a turbulent boundary layer at $Pr = 0.7$ (shown as data points).

where $\xi = y/\lambda$ and $f(1) = 0.5$. The experimental data are for the case of mass transfer where the diffusing cloud is submerged into a momentum boundary layer. The agreement between LST and the experiments is quite good. However, as pointed out by Shlien and Corrsin [30], the use of $C_{\max}$ and λ as scaling parameters is an insensitive way to determine similarity, since (i) two points on a monotonically decreasing curve are forced to coincide (the $\xi = 0$ and the $\xi = 1$ points), and (ii) the slope of this curve at $\xi = 0$ has to be zero.

Shlien and Corrsin measured the temperature profile behind a heated wire located at the wall of a turbulent boundary layer. Heat was supplied to the wire at a constant rate, so that their case is equivalent to the calculation of P_2 profiles using LST. The Prandtl number was 0.71 and the Reynolds number based on the displacement thickness of the turbulent boundary layer, δ_d, at the location of the wire was 6300. Shlien and Corrsin scaled their temperature results with the maximum temperature, similar to Poreh and Cermak, but they scaled the distance from the wall and the distance downstream from the source with the displacement thickness of the turbulent boundary layer. Fig. 2 presents a comparison of the LST results for $Pr = 0.7$ with the experimental results of Shlien and Corrsin. In order to calculate the appropriate length scale for the channel flow DNS, the assumption was made that the mean centerline velocity of the channel can be used in place of $\overline{U}_\infty$ for the calculation of the momentum boundary layer. The calculated value for the DNS is $\delta_d = 23.2$ and the Re for the DNS based on this length scale and the mean centerline velocity is 490. There is qualitative agreement for all cases, and quantitative agreement close to the wall and close to the source. Given the differences

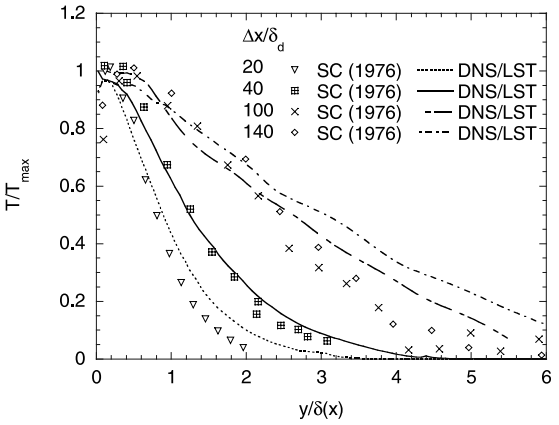

Fig. 2. Mean temperature profile downstream from a continuous line source at $Pr = 0.7$ using the DNS/LST method and comparison to measurements by Shlien and Corrsin (SC) [30] in a turbulent boundary layer.

in the problem setup (i.e. the experimental measurements were taken at a higher *Re* and in a developing turbulent boundary layer), the agreement is quite encouraging for the validity of the LST results.

Figs. 3(a) and (b) present the mean concentration profile downstream from the source as a function of *Pr* using the displacement thickness as a length scale. The value of δ_d for the velocity field does not change downstream of the heat source, so that scaling with the channel half-height *h* would result in similar plots. It is also seen in Fig. 3 that as the *Pr* increases the cloud is more concentrated close to the wall of the channel, as expected.

Figs. 4(a) and (b) present the ground level temperature downstream from the continuous source for low and high *Pr* runs, respectively. The values are normalized with the ground level temperature immediately downstream from the source (in the interval $0 < (x - x_0) < 5$) for $Pr = 1$. If one assumes a relation of the form

$$T_w = c_1(x - x_0)^{c_2}, \tag{12}$$

then Table 1 presents the values of the coefficients in this equation. Fig. 4(b) shows that for higher *Pr* there is a change in the slope of the line at long distances downstream from the source location. It appears that there are two zones of plume development, that become evident when the *Pr* increases. This phenomenon is not an end effect that arises at the front of the plume, simply because the front of the plume is even further downstream and has not been plotted in the figure. The observation of this second zone can be interpreted by keeping in mind that the behavior of a cloud of markers resulting from a continuous line source (plume of markers) is the result of the integrated behavior of a cloud of markers that was released instantaneously from a line source (puff of markers). It has been reported that the behavior of a puff in a channel flow can be distinguished in three zones: Zone I, where molecular diffusion dominates the dispersion, Zone II, which is the transition zone, and Zone III, where turbulent convection dominates the dispersion [31]. The extent of the first two zones depends on the *Pr*. In the transition zone, which becomes more pronounced as the *Pr* increases, markers "leak" out of the cloud and create a second area of high marker concentration downstream of the main cloud. The main cloud has been observed to be mostly located in the viscous wall region, so it moves downstream with low average velocity, while the "leaked" markers tend to be uniformly distributed across the channel, and move with the bulk velocity of the fluid. Considering now the case of a plume, the temperature profile downstream from the source is

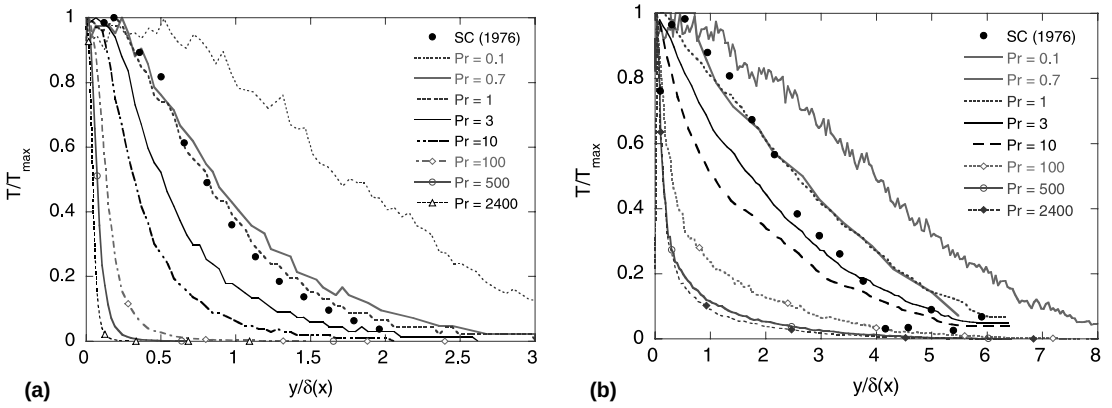

Fig. 3. Mean temperature or mean concentration profile downstream from a continuous line source using the boundary layer displacement thickness as length scale. Data by Shlien and Corrsin (SC) [30] are shown as dark circles: (a) $(x - x_0) = 20\delta_d$; (b) $(x - x_0) = 100\delta_d$.

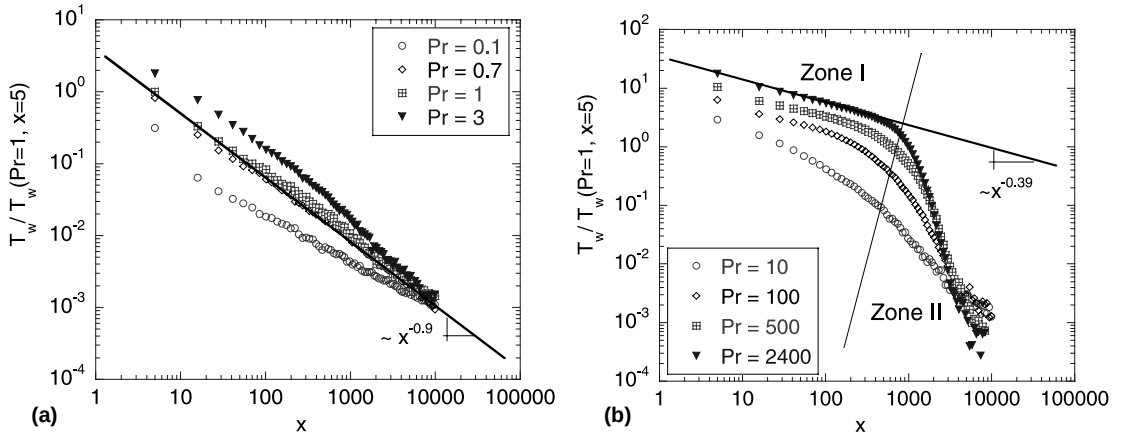

Fig. 4. Mean ground level temperature downstream from a continuous line source of heat at $Pr = 1$: (a) low Pr runs ($Pr \leqslant 3$); (b) high Pr runs ($Pr \geqslant 10$).

Table 1
Coefficients for the ground level temperature T_w vs. x correlation for the two Zones of plume development, when the ground level temperature is normalized with the ground level temperature immediately downstream from a $Pr = 1$ source

Pr	Zone I		Zone II	
	c_1^{I}	c_2^{I}	c_1^{II}	c_2^{II}
0.1	0.37	−0.645		
0.7	3.397	−0.86		
1	4.885	−0.89		
3	6.435	−0.786	43.428	−1.145
10	16.243	−0.800	474.97	−1.4145
100	12.798	−0.433	5.6×10^5	−2.209
500	18.934	−0.386	3.071×10^{10}	−3.5393
2400	32.366	−0.389	2.85×10^{12}	−4.1371

affected by different parts of the composing puffs of markers. Zone I of plume development is affected by puffs in their Zone I stage of development, and Zone II of plume development is affected by a collection of puffs that are in their Zones II and III of development. Table 1 also presents the coefficients in Eq. (12) for the second plume Zone. As the Prandtl number increases, the ground level concentration $T_w[(x - x_0) < 5]$ increases because the elementary puffs of markers that compose the plumes stay closer to the wall for a longer time.

The relation between the puff and the plume behavior can be further demonstrated by examining the reason for the clearly discernible Zone I of plume development at higher Pr. It has been found [31] that if we define a timescale for which the puff is 95% dominated by molecular diffusion (Brownian motion of the markers as predicted by Einstein's relation), then the Pr dependence of this timescale is $8.34Pr^{0.38}$. It has also been found that the mean puff position in this sub-region of Zone I is analogous to $(t^+ - t_0^+)^{3/2}$. For example, a puff for $Pr = 2400$ travels for a time of about $(t^+ - t_0^+) = 8.34\,2400^{0.38} = 160.56$ due to Brownian motion, and reaches on average a distance $\simeq 160.56^{3/2} = 2034$ downstream. A puff for $Pr = 100$ travels due to Brownian motion to a distance of about $x \simeq 332$ downstream from its source and a puff for $Pr = 1$ to a distance of about $x \simeq 24$. As the Pr decreases, this distance is smaller. Beyond this distance, the effects of convection first by viscous velocity and then by turbulence become important. The extent of this region of puff travel appears to be strongly correlated to the extent of Zone I of plume development, as seen in Fig. 4(b).

Batchelor [32] has developed a theory for the diffusion from sources in a turbulent boundary layer, based on the assumption that wall similarity applies to Lagrangian quantities. His theory predicted a dependence of the ground level concentration (or temperature) of the form $T_w \sim x^{-1}$. The present results for Zone I of plume development show that the ground level temperature downstream from the source declines with different rates depending on the Pr. The dependence is closer to the value predicted by Batchelor for $Pr \simeq 1$. As the Pr

increases, the dependence is described by the relation $T_w \sim x^{-0.4}$.

Batchelor's analysis did not address the issue of the effects of Pr and assumed that the thermal layer is within the velocity logarithmic layer. A basic assumption in the calculations for the asymptotic ground level concentration as $x \to \infty$ was that the shape of the puff (the distribution P_1) is similar at all times and that the length scale is the same in the y and in the x direction. This assumption makes sense for low Pr fluids and for the case of flow in a boundary layer, when the conceptual picture of a puff is the picture of a balloon that expands with time. However, as discussed briefly here and in more detail elsewhere [31], the high Pr puffs do not expand like a balloon, but exhibit three zones of development. Furthermore, the presence of the channel wall opposite to the wall that contains the source constricts the expansion of the puff in the y direction.

4.2. The case of a step change in the wall heat flux

The case of transport downstream from a step change in wall heat flux is considered in this section. It is a variation of the usually named "Graetz problem", which describes heat transfer from the wall of a vessel with constant heat flux [33]. Teitel and Antonia [9] have taken temperature measurements in a fully developed turbulent channel flow with a step change in the heat flux applied to one of the walls of the channel. The Reynolds number for these experiments in wall units was 180; it is comparable to the present DNS Reynolds number. Antonia et al. [34] have also measured the temperature field in a thermal layer that grows inside a turbulent boundary layer, which was subject to a small step change in surface heat flux. The Re of those experiments in wall units was 1500. Fig. 5 presents the calculated mean temperature profile downstream from the edge of the heated section of the channel wall calculated with LST, according to Eq. (10) for $Pr = 0.7$. The experimental measurements of Teitel and Antonia are presented for comparison, as well as the measurements of Antonia et al. for a long distance downstream from the step change in wall heat flux. The data of Fulachier (as were presented in reference [34]) for the case of a step change in the wall temperature of a boundary layer are also shown. The agreement between LST and experiments is quite good for the cases of $x/h = 7.6$, 21.4, 32.4 and good for the cases of $x/h = 17.1$ and 47.6. Teitel and Antonia's measurements show temperature profiles that are very close to each other for every two distances, i.e. almost the same for $x/h = 17.1$ and 21.4, and $x/h = 32.4$ and 47.6. Even the higher Re data appear to agree with the LST results. The profile predicted by Kader [35] using a semi-empirical formulation for a fully developed turbulent boundary layer is also presented in Fig. 5. The LST results appear to tend towards Kader's predictions at long distances downstream from the edge of the heated region.

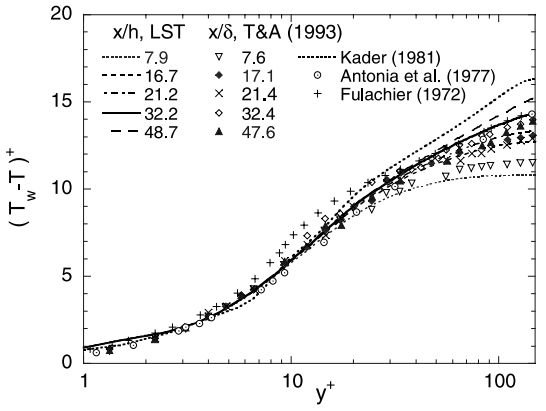

Fig. 5. Mean temperature profiles downstream from a step change in the heat flux from the wall of a channel. The lines are LST results and the points are measurements from Teitel and Antonia (TA) [9], Antonia et al. [34] and Fulachier.

Fig. 6 is a comparison of the development of the outer edge of the thermal layer for the case of $Pr = 0.7$ between experiments and the LST. The thermal layer thickness, δ_T, is defined following the suggestion of Antonia et al. [34] as the distance from the wall $y = \delta_T$ at which $(T - T_l) = 0.01(T_w - T_l)$. Given the different Re between the laboratory and the numerical experiments, and the fact that the laboratory data were obtained for the case of a thermal layer within a developing velocity boundary layer, the agreement is good.

The heat transfer coefficient can be calculated using Eq. (3). The calculation depends on the measurement

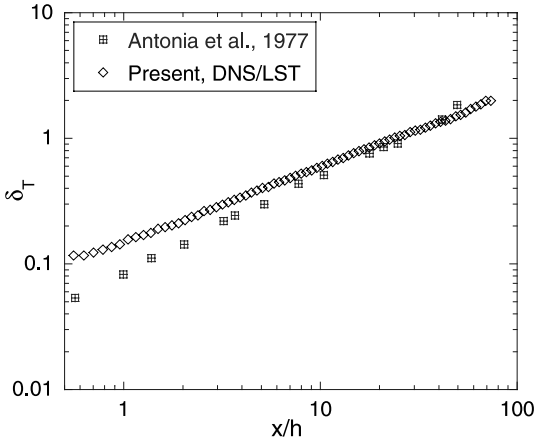

Fig. 6. Change of the thickness of the thermal layer, δ_T, with the distance downstream from the thermal entry region. The LST results are normalized with the channel half-height and the results of Antonia et al. [34] are normalized with the thickness of the velocity boundary layer.

of the gradient of the mean temperature (calculated through Eq. (10)) at the wall. Since the mean temperature is found at the center of a bin with the use of statistical methods, there is a need to have appropriately small bin widths near the wall and to extrapolate the temperature profile to the wall. The temperature profile inside the conductive transport sublayer is known to be $\bar{T}^+ = Pr\,y^+$. Inside the conductive wall sublayer, therefore, a linear extrapolation is accurate. It is necessary, however, to make sure that several bins lie within the conductive sublayer, whose thickness depends on the *Pr*.

The Nusselt number ratio $Nu(x)/Nu(x \to \infty)$ as a function of the distance downstream from the heated edge is presented in Fig. 7 for the different *Pr* fluids examined. As the *Pr* increases, the value of the Nusselt number ratio decreases for the same position downstream from the location of the step change in the wall heat flux, x_0. This type of behavior is in agreement with Eulerian results obtained numerically for the entry region of a circular pipe for $Pr = 0.02$, 0.72 and 14.3 with uniform wall heat [36]. The Lagrangian interpretation of this observation is related to the fact that the transfer of heat follows the expansion of the heat marker cloud. The driving force for heat transport between two locations in the Lagrangian sense is the difference in the number of markers present in these two locations. The *Nu* is proportional to the heat transfer coefficient, which is inversely proportional to the driving force for transfer when the heat flux remains constant. At high *Pr*, the cloud of markers is mostly located close to the wall of the channel. This configuration persists for all distances downstream from x_0 and thus the driving force is similar for all distances downstream from x_0. For a low *Pr* cloud, the markers leave the viscous wall layer, due to large molecular jumps, and the cloud becomes more disperse in the vertical direction as the distance $(x - x_0)$ increases. Therefore, for low *Pr* the cloud presents a changing configuration as it convects downstream from x_0, which results in significant changes in the Nusselt number.

It is also important to note that the Nusselt number ratio reaches the value of one at shorter distances downstream from the edge of the thermal layer as the *Pr* becomes higher. This means that the plumes at higher *Pr* affect the downstream wall temperature over a smaller distance from the continuous line source. For example, the Nusselt number ratio changes within a short distance $(x/h < 5)$ for high Prandtl numbers ($Pr = 2400$), and this distance agrees well with the length of Zone I of a plume with the same Prandtl number. The value of T_w downstream from a plume (see Fig. 4) can be used as a measure of the relative effect that sources at different distances upstream from a point at the wall have on the local T_w for the case of a step change in heat flux. This relative effect is shown in Fig. 4 to be strong for sources close to a point and weak for sources away from it as the *Pr* increases. For low *Pr*, the relative effect of sources at different distances from a point decreases in a more uniform way.

In order to provide more information regarding the applicability of the Lagrangian method in different cases, the LST results are compared with experimental results for the case of a step change in the wall temperature. Johnson and Whippany [37] and Hoffmann and Perry [38] have conducted such experiments in wind tunnels and h^+ equal to 2000 and 3000, respectively. The thermal layer was under development within a developing velocity boundary layer in both of these experiments. Fig. 8 presents the Standon number as a function of the distance downstream from the step change in wall

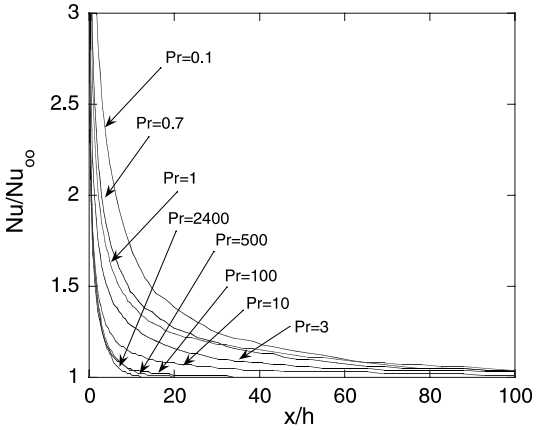

Fig. 7. Change of the Nusselt number ratio with the distance downstream from the thermal entry region.

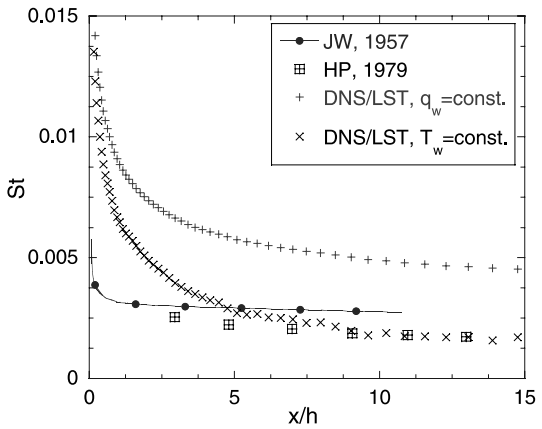

Fig. 8. Variation of the heat transfer coefficient as a function of the distance downstream from the thermal entry region.

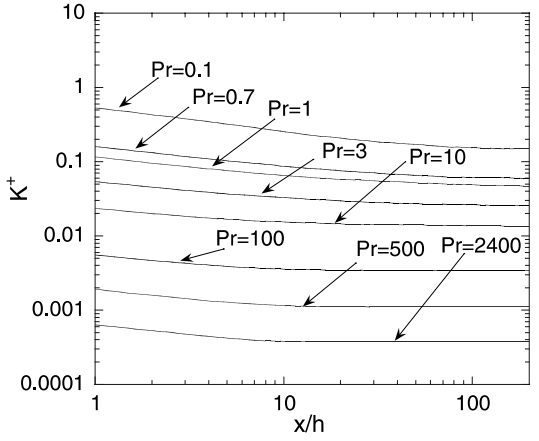

Fig. 9. Variation of the Standon number as a function of the distance downstream from the thermal entry region that results from a step change in the wall temperature and from a step change in the wall heat flux ($Pr = 0.7$). The experimental results are from Johnson and Whippany (JW) [37] and Hoffmann and Perry (HP) [38].

Table 2
Coefficients for the K^+ vs. Pr correlation for $Pr \geqslant 100$ ($K^+ = APr^m$)

x/h	A	m
1	0.1205	−0.670
2	0.1053	−0.677
5	0.0950	−0.694
10	0.0915	−0.704
25	0.0871	−0.701
50	0.0853	−0.698
100	0.0847	−0.698

temperature. The distance is normalized with the channel half-height for all cases, experimental and numerical. The Lagrangian results were obtained by keeping the number of markers at the wall of the channel constant. The use of weight functions to account for the contribution of sources upstream from each point was necessary. The Standon number for a thermal region due to a step change in wall heat flux is also shown in the same figure.

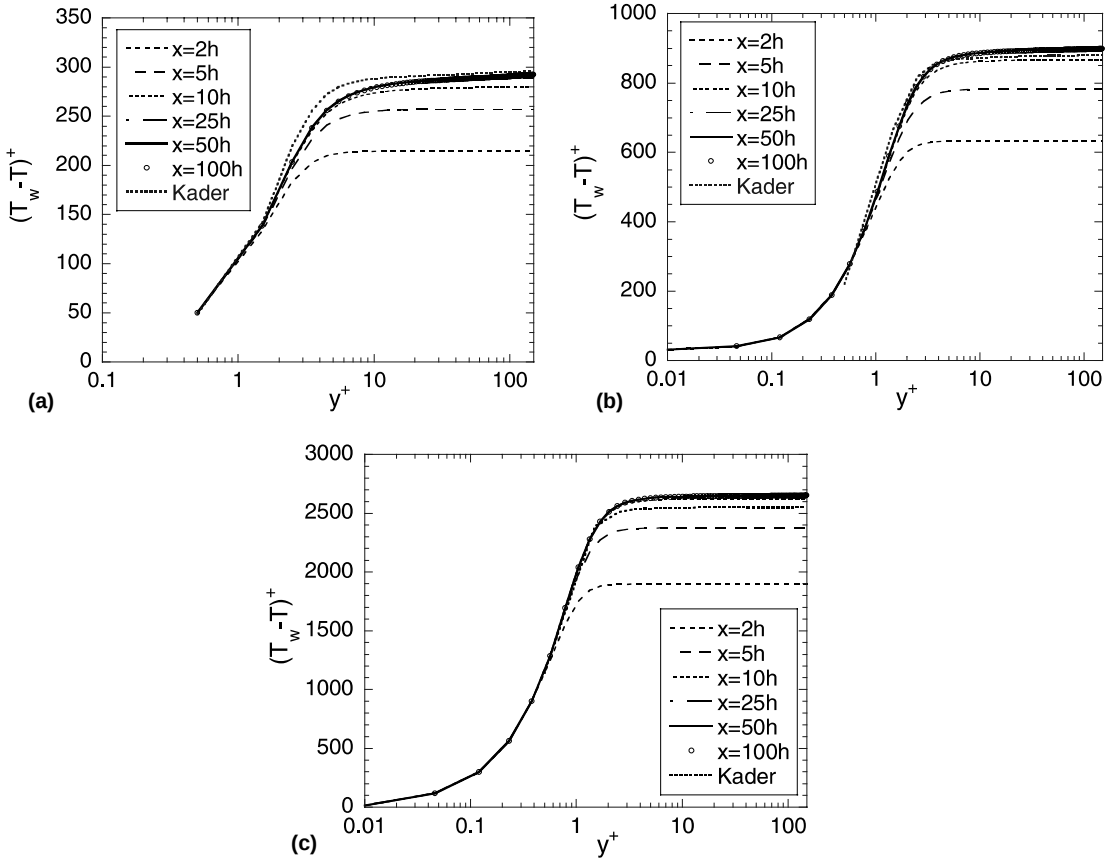

Fig. 10. Mean temperature at different distances downstream from a step change in wall heat flux: (a) $Pr = 100$; (b) $Pr = 500$; (c) $Pr = 2400$.

The actual heat transfer coefficient as a function of the distance downstream from x_0 for different Pr is presented in Fig. 9. The values decrease with Pr for every case. The Lagrangian interpretation is provided in the discussion above. The heat transfer coefficient is inversely proportional to the driving force (see Eq. (2)) and therefore smaller when the cloud of markers is more uniformly dispersed in the direction of transfer. At low Pr, this is the case more so than for high Pr and therefore the heat transfer coefficient is higher. Table 2 presents the parameters A and m (see Eq. (4)) for the dependence of the heat transfer coefficient on the molecular Pr of the fluid at different distances downstream from the point of step change in heat flux. At long distances downstream from point x_0, the relation goes to

$$K^+ = 0.085Pr^{-0.70} \tag{13}$$

for the high Pr cases ($Pr \geqslant 100$). The value of the exponent is different than the Deissler asymptotic prediction of $K^+ \sim Pr^{-3/4}$ or the Sieder–Tate prediction $K^+ \sim Pr^{-2/3}$, but is closer to the value measured by Shaw and Hanratty [11] (for $700 < Sc < 33,700$, $K^+ \sim Sc^{-0.704}$) and the value measured by Incropera et al. [21] (for $0.7 < Pr < 25$, $K^+ \sim Pr^{-0.72}$). This issue has both theoretical significance, because the value of the exponent depends on the asymptotic dependence of the eddy conductivity close to the wall on the distance from the wall, and practical interest, because such correlations are implemented in the development of models for turbulent transport. Further investigation with a wider range of high Pr runs is needed in order to provide a more definite statement regarding the value of the exponent.

Figs. 10(a)–(c) present the mean temperature in wall units downstream from the point of the step change in wall heat flux for the high Pr fluids calculated with the LST. The temperature profile resulting from Kader's semi-empirical formula is also shown as a reference. The development of the temperature profile is mostly taking place within a short distance from the edge of the heat flux region.

5. Discussion and conclusions

Direct Numerical Simulation of turbulent heat transfer in the Eulerian framework has been used in the literature to gain insights into the mechanism of wall transport. However, restrictions in the size of the computations have not allowed the study of an extensive range of Prandtl number fluids, with more difficulties arising for the cases of higher Prandtl. The present work utilized the Lagrangian Scalar Tracking method to develop Eulerian results for the case of heat transfer from a continuous line source at the wall of a turbulent flow channel and for the case of a modified Graetz problem, where a step change in wall heat flux takes place. The results demonstrated the validity of LST as a method for obtaining quantitative information for heat transfer problems. Qualitative agreement with experimental measurements was observed in all cases studied and quantitative agreement was observed in most cases studied. Of particular interest is the demonstration that it is possible to use this technique at very high Pr, where the application of Eulerian DNS is not feasible.

A Lagrangian analysis was used to interpret the Eulerian results. The interpretation was based on the fact that the dispersion of heat markers from a source at the wall is a function of the time the markers have been in the field and of the Prandtl number. The mean temperature profile downstream from a continuous line source was calculated as well as the ground level value of the mean temperature. The dependence of Nu on the distance from the thermal entry region for different Pr was examined as well as the dependence of the heat transfer coefficient on this distance. Also, the dependence of turbulent transport properties on the molecular Pr was studied.

The next challenge for LST is to develop a methodology for obtaining second order statistics for the temperature or the concentration field. It will be quite interesting to compare such results with recent theories for turbulent heat transport [39,40] that predict the turbulent transport properties based on differential models for the complete range of Pr. These theoretical advances utilize the local turbulent shear stress and the local heat flux density instead of the heat flux density based on the friction velocity at the wall. The ability of LST to simulate transport at different Pr suggests that it is very appropriate for studies in this direction. Runs with the use of many more markers (currently underway in our laboratory) will be needed for such an analysis. Furthermore, a model that predicts the behavior of the probability function P_1, which is the building block for the Lagrangian reconstruction of the Eulerian measurements, as a function of the Prandtl number and the time elapsed since the marker release is needed for the development of predictive models of turbulent transport from the wall using the present approach.

Acknowledgements

Access to the Lagrangian database of Professor Thomas J. Hanratty's group at the University of Illinois is gratefully acknowledged. This work was partially supported by the National Computational Science

Alliance under CTS990021N and utilized the NCSA Convex C3880, the NCSA HP-Convex Exemplar SPP-2000 and the NCSA SGI/CRAY Origin2000. The author also acknowledges the support of the Research Council at the University of Oklahoma through the Junior Faculty Research award.

References

[1] N. Kasagi, N. Shikazono, Contribution of direct numerical simulation to understanding and modeling turbulent transport, Proc. R. Soc. London A 451 (1995) 257–292.
[2] J. Kim, P. Moin, Transport of passive scalars in a turbulent channel flow, in: Andre, Cousteix, Durst, Launder, Schmidt, Whitelaw (Eds.), Turbulent Shear Flows, vol. 6, Springer, Berlin, 1989, pp. 85–96.
[3] S.L. Lyons, T.J. Hanratty, J.B. McLaughlin, Direct numerical simulation of passive heat transfer in a turbulent channel flow, Int. J. Heat Mass Transfer 34 (4/5) (1991) 1149–1161.
[4] N. Kasagi, Y. Tomita, A. Kuroda, Direct numerical simulation of passive scalar field in a turbulent channel flow, Trans. ASME 114 (1992) 598.
[5] H. Kawamura, K. Ohsaka, H. Abe, K. Yamamoto, DNS of turbulent heat transfer in channel flow with low to medium-high Prandtl number fluid, Int. J. Heat Fluid Flow 19 (1998) 482–491.
[6] Y. Na, D.V. Papavassiliou, T.J. Hanratty, The effect of Prandtl number on turbulent temperature fields, Int. J. Heat Fluid Flow 20 (3) (1999) 187–195.
[7] I. Tiselj, E. Pogrebnyak, L. Changfeng, A. Mosyak, G. Hetsroni, Effects of wall boundary condition on scalar transfer in a fully developed turbulent flume, Phys. Fluids 13 (4) (2001) 1028–1039.
[8] M. Teitel, R.A. Antonia, Heat transfer in fully developed turbulent channel flow: comparison between experiment and direct numerical simulations, Int. J. Heat Mass Transfer 36 (6) (1993) 1701–1706.
[9] M. Teitel, R.A. Antonia, A step change in wall heat flux in a transfer in turbulent channel flow, Int. J. Heat Mass Transfer 36 (6) (1993) 1707–1709.
[10] D.V. Papavassiliou, T.J. Hanratty, Transport of a passive scalar in a turbulent channel flow, Int. J. Heat Mass Transfer 40 (6) (1997) 1303–1311.
[11] D.A. Shaw, T.J. Hanratty, Turbulent mass transfer to a wall for large Schmidt numbers, AIChE J. 23 (1) (1997) 28–37.
[12] A. Einstein, Uber die von der molekular–kinetischen Theorie der Warme geforderte Bewegung von in ruhenden Flussigkeiten suspendierten Teilchen, Ann. Phys. 17 (1905) 549.
[13] G.I. Taylor, Diffusion with continuous movements, Proc. London Math. Soc. 24A (1921) 196–212.
[14] P.G. Saffman, On the effect of the molecular diffusivity in turbulent diffusion, J. Fluid Mech. 8 (1960) 273–283.
[15] T.J. Hanratty, Heat transfer through a homogeneous isotropic field, AIChE J. 2 (1) (1956) 42–45.
[16] D.L. Eckelman, T.J. Hanratty, Interpretation of measured variations of the eddy conductivity, Int. J. Heat Mass Transfer 15 (1972) 2231–2239.
[17] M. Poreh, J.E. Cermak, Study of diffusion from a line source in a turbulent boundary layer, Int. J. Heat Mass Transfer 7 (1964) 1083–1095.
[18] M. Poreh, K.S. Hsu, Diffusion from a line source in a turbulent boundary layer, Int. J. Heat Mass Transfer 14 (1971) 1473–1473.
[19] J.E. Fackrell, A.G. Robins, Concentration fluctuations and fluxes in plumes from point sources in a turbulent boundary layer, J. Fluid Mech. 117 (1982) 1–26.
[20] M.R. Raupach, B.J. Legg, Turbulent dispersion from an elevated line source: measurements of wind-concentration moments and budgets, J. Fluid Mech. 136 (1983) 111–137.
[21] F.P. Incropera, J.S. Kerby, D.F. Moffatt, S. Ramadyani, Convection heat transfer from discrete heat sources in a rectangular channel, Int. J. Heat Mass Transfer 29 (7) (1986) 1051–1058.
[22] P. Paranthoen, A. Fouari, A. Dupont, J.C. Lecordier, Dispersion measurements in turbulent flows (boundary layer and plane jet), Int. J. Heat Mass Transfer 31 (1) (1988) 153–165.
[23] K. Kontomaris, Point source dispersion in a direct numerical simulation of turbulent channel flow, Ph.D. Dissertation, University of Illinois, Urbana, 1991.
[24] K. Kontomaris, T.J. Hanratty, Effect of molecular diffusivity on point source diffusion in the center of a numerically simulated turbulent channel flow, Int. J. Heat Mass Transfer 37 (1994) 1817–1828.
[25] S.S. Ponoth, J.B. McLaughlin, Numerical simulation of mass transfer for bubbles in water, Chem. Eng. Sci. 55 (2000) 1237–1255.
[26] S.L. Lyons, T.J. Hanratty, J.B. McLaughlin, Large-scale computer simulation of fully developed turbulent channel flow with heat transfer, Numer. Methods Fluids 13 (1991) 999–1028.
[27] A. Guenther, D.V. Papavassiliou, M.D. Warholic, T.J. Hanratty, Turbulent flow in a channel at low Reynolds number, Exp. Fluids 25 (1998) 503–511.
[28] K. Kontomaris, T.J. Hanratty, J.B. McLaughlin, An algorithm for tracking fluid particles in a spectral simulation of turbulent channel flow, J. Comput. Phys. 103 (1992) 231–242.
[29] J.E. Cermak, Lagrangian similarity hypothesis applied to diffusion in turbulent shear flow, J. Fluid Mech. 15 (1963) 29–64.
[30] D.J. Shlien, S. Corrsin, Dispersion measurements in a turbulent boundary layer, Int. J. Heat Mass Transfer 19 (3) (1976) 285–295.
[31] D.V. Papavassiliou, Scalar dispersion from an instantaneous line source at the wall of a turbulent channel for medium and high Prandtl number fluids, Int. J. Heat Fluid Flow 23 (2) (2002) 161–172.
[32] G.K. Batchelor, Diffusion from sources in a turbulent boundary layer, Arch. Mech. Stos. 3 (6) (1964) 661–670.
[33] R.B. Bird, W.E. Stewart, E.N. Lightfoot, in: Transport Phenomena, Willey and Sons, New York, 1960, p. 361.

[34] R.A. Antonia, H.Q. Danh, A. Prabhu, Response of a turbulent boundary layer to a step change in surface heat flux, J. Fluid Mech. 80 (1977) 153–177.
[35] B.A. Kader, Temperature and concentration profiles in fully turbulent boundary layers, Int. J. Heat Mass Transfer 29 (9) (1981) 1541–1544.
[36] T. Cebeci, P. Bradshaw, in: Physical and Computational Aspects of Convective Heat Transfer, Springer-Verlag, New York, 1984, p. 229.
[37] D.S. Johnson, N.J. Whippany, Velocity, temperature, and heat-transfer measurements in a turbulent boundary layer downstream of a stepwise discontinuity in wall temperature, J. Appl. Mech. 24 (March) (1957) 2–8.
[38] P.H. Hoffman, A.E. Perry, The development of turbulent thermal layers on flat plates, Int. J. Heat Mass Transfer 22 (1979) 39–46.
[39] S.W. Churchill, Progress in the thermal sciences: AIChE Institute lecture, AIChE J. 46 (9) (2000) 1704–1722.
[40] B. Yu, H. Ozoe, S.W. Churchill, The characteristics of fully developed turbulent convection in a round tube, Chem. Eng. Sci. 56 (2001) 1784–1800.